

Plasmon control of molecules luminescence in the structure of an adsorbed polymer chain on the charged spherical nanoparticle surface

© M.G. Kucherenko, A.P. Rusinov, N.Yu. Kruchinin

Center of Laser and Information Biophysics, Orenburg State University, Orenburg, Russia

e-mail: sano232@mail.ru

Received April 22, 2024

Revised May 28, 2024

Accepted May 28, 2024

The formation of a stable conformational structure of a polyampholytic macromolecule during its adsorption on the surface of a plasmonic nanoparticle is considered. It is shown that the placement of an additional electric charge on a nanoparticle changes the architecture of the polymer superstructure, the degree of its looseness and, consequently, the order of distancing (localization) of phosphor molecules associated with the macrochain. This leads to a change in the emissivity of the system due to a change in the mode of plasmon assisting radiation transitions. This effect makes it possible to consider charge transfer to a nanoparticle as a factor of supramolecular structural control of the radiative properties of hybrid metal-polymer composites in functional nanodevices for various purposes. The performed molecular dynamic modeling of some polyampholytic polypeptides on a charged metal nanoparticle demonstrates the swelling of the polymer shell, which is structured in layers depending on the charge sign of the amino acid residue, and its thickness depends on the distance between the charged links in the macromolecule.

Keywords: luminescence of molecules, polypeptide, adsorption, metal nanoparticle, plasmon resonance, polyampholyte.

DOI: 10.61011/EOS.2024.05.59124.6310-24

Introduction

Plasmonic nanoparticles (NP) with biogenic polymer chains adsorbed on their surface are widely used as nanometer-scale probes in biomedicine and in various chemical sensors and nanoelectronics sensors [1–8]. Controlled performance modification of such nanosystems for creation of luminescent sensors with adjustable parameters is of special interest. Exposure of electric dipoles of polyampholyte units to electric charges distributed over the NP surface may be considered as one of the mechanisms of permolecular structural control over nanodevices intended for various purposes.

Thus, when an additional electric charge is applied to NP or when NP is polarized in external static or variable electric field, areas with like-sign or unlike-sign charges are formed on the particle surface. Electric interaction between these surface charge regions and polyampholyte or polyelectrolyte macrochains will change considerably the shape and density of a polymer shell (crown) that envelopes NP [9–14]. For metallic NP with different electric charges both in magnitude and sign, different conformation structures of adsorbed polyampholyte macrochains will be formed with small functional molecules and atomic groups with desired electronic and optoelectronic properties easily introduced in them [15,16]. If organic dyes are used as such inclusions, then the structural variations of the macromolecular crown will change both the distance between the molecules themselves and the distance between the molecules and

plasmonic NP. Since various electron excitation deactivation channels of photoactive molecules depend considerably on the spatial arrangement of the molecules with respect to NP [17,18], then charge generation, that induces chain restructuring, on the NP surface may be considered as a method of control over the luminescent signal efficiency of this hybrid system.

Thus, the objective of this study is to investigate the changes in luminescent spectral properties of a „molecule-NP“ two-particle system depending on the electric charge of a plasmonic NP on which a polyampholyte macrochain containing photoactive molecules is absorbed.

Polyampholyte adsorption on a charged spherical NP

Polymer chain is attracted to an electrically neutral NP by means of the Van der Waals forces. The potential energy of interaction between the chain unit and uncharged spherical NP with the radius R (in case of the initial 6–12 Lennard-Jones pair potential for the intermolecular interaction between the unit atoms and NP) is written as ($r > R$) [1]

$$V_{9-3}(r) = \frac{\pi D n_0 r_m^6}{6r} \left(\frac{r_m^6}{60} \left[\frac{9R+r}{(R+r)^9} - \frac{9R-r}{(R-r)^9} \right] - \left[\frac{3R+r}{(R+r)^3} - \frac{3R-r}{(R-r)^3} \right] \right). \quad (1)$$

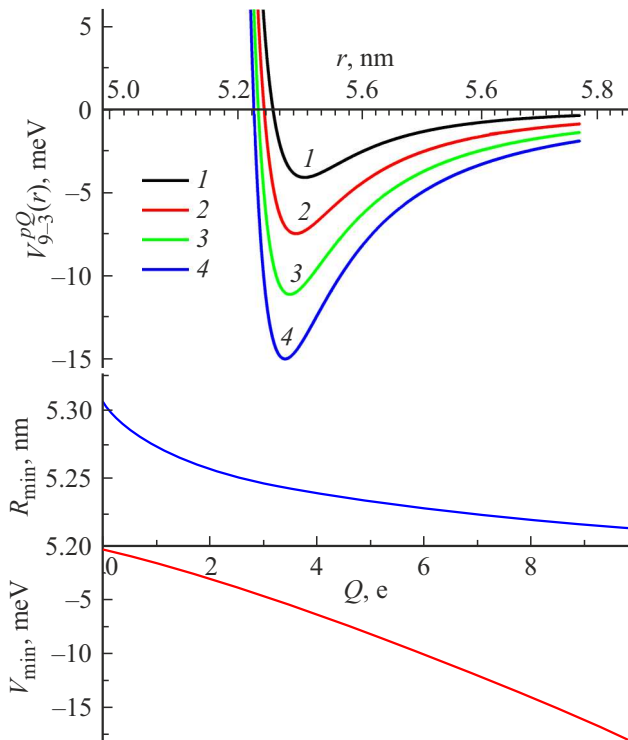


Figure 1. Radial potential distribution of a neutral (1) and charged (2–4) NP with various absolute values of the NP charge Q : 2 — $3e$, 3 — $6e$, 4 — $9e$ and dependence of the potential well valley R_{\min} and depth V_{\min} with the increase in the NP charge. $R_{\text{NP}} = 5 \text{ nm}$, $D = 0.2kT$, $r_m = 0.4 \text{ nm}$.

Here, D and r_m are parameters of the 6–12 Lennard-Jones potential, n_0 is the concentration of NP metal atoms.

In case of a charged NP with spherically symmetrically distributed charge Q and a polyampholyte chain with the dipole moment \mathbf{p} of its unit, a macrochain monomer interaction potential is added to the adsorption potential (1)

$$V_{pQ}(r) = -(\mathbf{pr})Q/r^3$$

with the Coulomb field of charged NP:

$$V_{9-3}^{pQ}(r) = V_{9-3}(r) + V_{pQ}(r) = V_{9-3}(r) - Q \frac{(\mathbf{pr})}{r^3}. \quad (2)$$

Figure 1 shows that as the NP charge increases from 0 to $9e$, the potential valley V_{\min} shifts a little towards the NP surface, and the potential well depth increases. This results in an increase in the radial distribution amplitude of the chain units near the NP surface. In this case the density of units may be calculated most simply in the Boltzmann approximation

$$n(r) \sim \exp[-V_{9-3}^{pQ}(r)/kT]$$

on the basis of the potential $V_{9-3}^{pQ}(r)$ calculated by expression (2). However, such approach does not consider many important polymer properties, for example, the chain unit

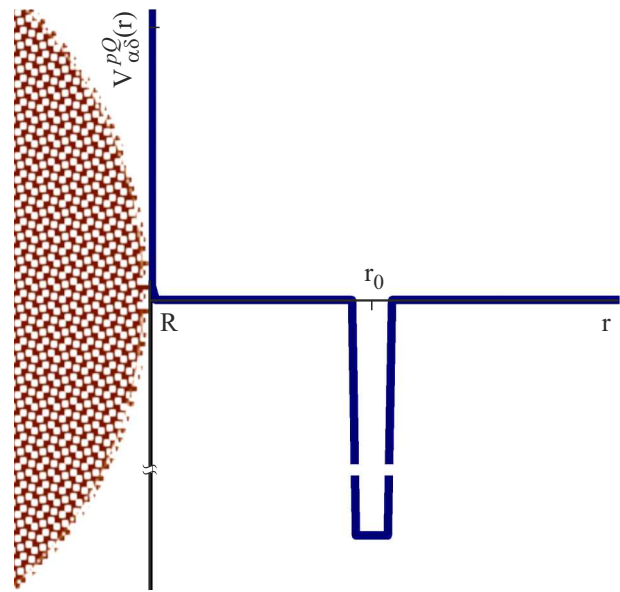


Figure 2. View of the model adsorption potential of the NP surface approximated by the Dirac delta function.

dimensions, connectivity of primary structure units, etc., that define conformational entropy effects.

In [19,20], an approach is offered to describe the equilibrium structure of the adsorbed macrochain with the length of units a at the absolute temperature T on the basis of the conformational function $\psi(\mathbf{r})$ satisfying the isomorphic nonlinear Schrödinger equation,

$$\frac{a^2kT}{6} \nabla^2 \psi(\mathbf{r}) = [V(\mathbf{r}) - \varepsilon] \psi(\mathbf{r}). \quad (3)$$

The spatial distribution of the local density $n(\mathbf{r})$ of chain units in [19] is determined by the squared function $\psi_0(\mathbf{r})$ meeting the minimum eigenvalue ε_0 of the discrete spectrum $\{\varepsilon_n\}$: $n(\mathbf{r}) = \psi_0^2(\mathbf{r})$.

Like in [21,22], for the uncharged spherical NP, replace the potential $V_{9-3}(r)$ (1) with a simple model $V_{\alpha\delta}^\infty(r) = V_\infty(R) - \alpha\delta(r - r_0)$ „solid wall–delta-functional well“ potential (Figure 2) [21,22] where point r_0 of the delta-functional well localization coincides with the potential well bottom radius (1), and the model potential parameter α is proportional to the potential depth $V_{9-3}(r_0)$ in the potential valley. In this case, the radial functions $\psi(r) = F_0(r)$ are defined inside the spherical layer $R < r < r_0$ and in the conjugate area $r > r_0$:

$$\begin{cases} F_0^I(r) = A_0 \left[\frac{I_{1/2}(q_0r)}{\sqrt{r}} - \frac{I_{1/2}(q_0R)}{K_{1/2}(q_0R)} \frac{K_{1/2}(q_0r)}{\sqrt{r}} \right], & R < r < r_0, \\ F_0^{II}(r) = A_0 \left[\frac{I_{1/2}(q_0r_0)}{K_{1/2}(q_0r_0)} - \frac{I_{1/2}(q_0R)}{K_{1/2}(q_0R)} \right] \frac{K_{1/2}(q_0r)}{\sqrt{r}}, & r_0 < r < \infty, \end{cases} \quad (4)$$

where $I_{1/2}(q_0r)$ and $K_{1/2}(q_0r)$ are the modified Bessel functions of the first and second kind with a semi-integral index and eigenvalue. $q_0^2 = -\frac{6\varepsilon_0}{a^2kT}$.

Transcendental equation

$$\frac{a^2kT}{6ar_0} = I_{1/2}(q_0r_0)K_{1/2}(q_0r_0) - K_{1/2}^2(q_0r_0) \frac{I_{1/2}(q_0R)}{K_{1/2}(q_0R)}. \quad (5)$$

makes it possible to determine the eigenvalue q_0 and also the single discrete spectrum level ε_0 together with it.

Addition of the charged NP potential $V_{pQ}(r) = -(\mathbf{pr})Q/r^3$ to composition (2) results in the model potential

$$V_{\alpha\delta}^{pQ}(r) = V_{\infty}(R) - \alpha\delta(r - r_m) - pQ/r^2,$$

for which and analytical solution of the Grosberg-Khokhlov equation may be obtained as written for the configuration function $F_0(r) \sim \psi_0(r)$ as, for example, in [12].

For the spherically symmetric case when the dipole moments of the chain units in equilibrium are arranged along the electric field strength vector $\mathbf{E} = \mathbf{r}Qr^{-3}$, the potential

$$V_{\alpha\delta}^{pQ}(r) = V_{\alpha\delta}^{\infty}(r) - pQ/r^2$$

loses its dependence on the dipole orientation angle. Introducing a new radial function $\chi(r)$ by substituting $F_0(r) = \chi(r)/\sqrt{r}$, we get the following equation for it

$$\chi'' + \frac{1}{r}\chi' - \left(q_0^2 + \frac{(1/4 - \gamma)}{r^2}\right)\chi(r) = 0, \quad (6)$$

where

$$q_0^2 = -\frac{6|\varepsilon_0|}{a^2kT}, \quad \gamma = -\frac{6p(|Q|)}{a^2kT}.$$

Note that equation (6) is the Bessel equation and when its solution

$$\chi(r) = AI_{\nu}(q_0r) + BK_{\nu}(q_0r)$$

may be represented by a set of modified Bessel functions of the first kind $I_{\nu}(q_0r)$ and second kind $K_{\nu}(q_0r)$ with index $\nu = \sqrt{1/4 - \gamma}$. The radial functions $F_0^I(r)$, $F_0^{II}(r)$ for two regions (near-surface $R < r < r_0$ and peripheral $r > r_0$) will be defined by expressions similar to equations (4) for the uncharged spherical NP, but with the Bessel function index $\nu = \sqrt{1/4 - \gamma}$ — a quantity reflecting a degree of interaction between the NP charge and polyampholyte unit dipole:

$$\begin{cases} F_0^I(r) = A \left[\frac{I_{\nu}(q_0r)}{\sqrt{r}} - \frac{I_{\nu}(q_0R)}{K_{\nu}(q_0R)} \frac{K_{\nu}(q_0r)}{\sqrt{r}} \right], & R < r < r_0 \\ F_0^{II}(r) = A \left[\frac{I_{\nu}(q_0r_0)}{K_{\nu}(q_0r_0)} - \frac{I_{\nu}(q_0R)}{K_{\nu}(q_0R)} \right] \frac{K_{\nu}(q_0r)}{\sqrt{r}}, & r_0 < r < \infty \end{cases} \quad (7)$$

It is easy to see that with $\gamma \rightarrow 0$, $\nu = 1/2$ and equations (7) go into expressions (4) found before for the uncharged spherical NP.

General transcendental equation for eigenvalues q_l

$$\frac{a^2kT}{6ar_0} = I_{l+1/2}(q_l r_0)K_{l+1/2}(q_l r_0) - K_{l+1/2}^2(q_l r_0) \frac{I_{l+1/2}(q_l R)}{K_{l+1/2}(q_l R)}, \quad (8)$$

makes it possible to determine q_l for each integral index l , and the single discrete spectral level ε_l in the delta-functional well together with it.

Squared radial function $F_0(r)$ defines the density of units $n(r) = F_0^2(r)$. Comparison of the distributions (Figure 3, a–c) calculated using different models shows their good agreement on the outside of the potential well with $r > r_0$ and the expected differences on the inside of the potential well ($r \leq r_0$) due to the different form of potential used in these models. The calculations for both models show that as the charge on NP grows distribution of the polyampholyte chain units becomes more compact and is contained in the potential well valley. Whereas in the Boltzmann approximation of free point units, offset of the unit distribution peak towards the NP surface is observed due to the shift of the potential valley $V_{9-3}^{pQ}(r)$ (Figure 1, 2), and the analytical model of the polymer chain resulting in expressions (6)–(8) almost ignores this effect.

To include the density distribution shift into the analytical model, a formal approach is proposed where the potential valley point r_0 is calculated for the charged NP case

$$V_{9-3}^{pQ}(r) = V_{9-3}(r) + V_{pQ}(r),$$

and only after this a delta function from the

$$V_{\alpha\delta}^{\infty}(r) = V_{\infty}(R) - \alpha\delta(r - r_0)$$

„solid wall–delta-functional well“ potential combination is placed in this point. A change in the NP charge Q results in the potential valley point offset and increase of the potential valley point depth, this data is included in r_0 and α of the model potential. The radial conformational functions $F_0^I(r)$, $F_0^{II}(r)$ are used as (4), rather than as (7). Figure 3, d shows good agreement of the calculations conducted in the Boltzmann approximation and using the formal analytical model.

Molecular-dynamic modeling of the conformational changes in polyampholytes on the charged metallic NP surface

Molecular-dynamic (MD) modeling of polyampholyte polypeptides on the surface of a charged gold NP with a radius of 1.5 nm was performed using NAMD 2.14 software suite [23]. NP atoms remained fixed during modeling. For polypeptides, the CHARMM22 force field [24] was used and the interaction with the gold NP was described by the Lennard-Jones potential parametrized in [25]. The Van der Waals potential was cut at a distance of 1.2 nm using the smoothing function between 1.0 nm and 1.2 nm. Electrostatic interactions were calculated directly at a distance of 1.2 nm, the „particle–mesh“ Ewald (PME) method [26] with a mesh size of 0.11 nm was used for greater distances. All molecular system was placed in a cube with edges 20 nm filled with the TIP3P water molecules [27].

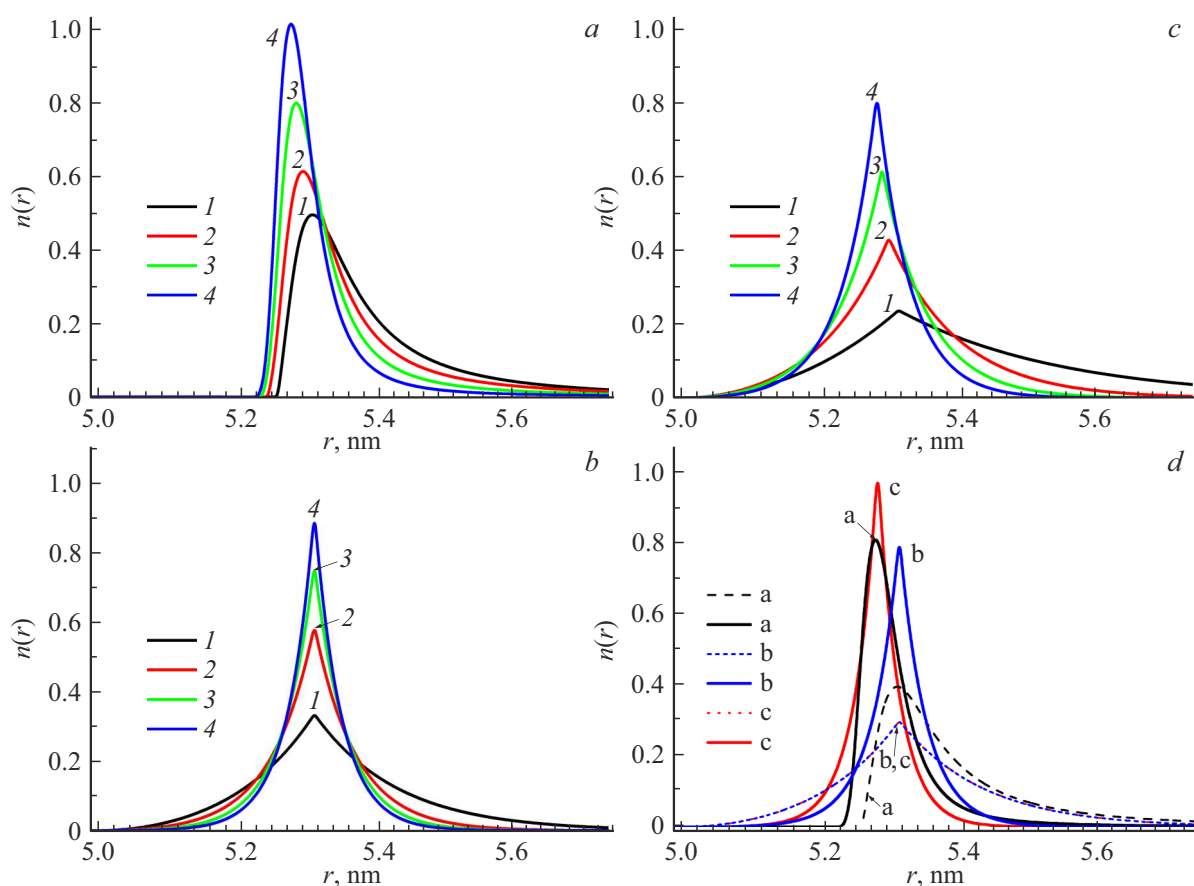


Figure 3. Radial distribution of the polyampholyte chain on the surface of the neutral NP (1) and charged NP with various absolute values of the NP charge Q : 2 — $3e$, 3 — $6e$, 4 — $9e$. (a) The Boltzmann approximation, (b) model according to equations (7), (c) formal model according to equations (4), (d) comparison of models for the NP charge: $9e$ (solid curves) and zero charge (dashed curves). $R_{NP} = 5$ nm, $D = 0.2kT$, $r_m = 0.4$ nm.

The following polyampholyte polypeptides were addressed:

1) polypeptide P1 — $(ADA_2RA)_{50}$ consisting of 300 amino-acid residues with 200 Ala (A) units with uniformly distributed 50 Asp units (D, charge $-1e$) and 50 Arg units (R, charge $+1e$);

2) polypeptide P2 — $(A_2DA_4RA_2)_{30}$ consisting of 240 Ala units, 30 Asp units and 30 Arg units;

3) polypeptide P3 — $(A_4R_2A_8D_2A_4)_{20}$ consisting of 320 Ala units with uniformly distributed 20 pairs of Asp units and 20 pairs of Arg units;

4) polypeptide P4 — $A_8(A_8D_2A_{16}R_2A_8)_8A_8$ consisting of 304 amino-acid residues with 272 Ala units with uniformly distributed 8 pairs of Asp units and 8 pairs of Arg units.

MD modeling was conducted at a constant temperature (Berendsen thermostat) during several nanoseconds: first, the temperature was set to 900 K and to -300 K on the final path segment. To control the achievement of equilibrium conformations, the change in the rms distance between the polypeptide atoms in various conformations (RMSD) was monitored.

At the first stage, three conformational structures were obtained for each given polypeptide on the uncharged NP surface that were further used as start structures for MD modeling on the charged gold NP surface. The NP surface was charged by assigning partial charges to the atoms on the NP surface. The following surface charge densities of the spherical NP were obtained: $\sigma_{\pm 0.05} \approx \pm 1e/nm^2$, $\sigma_{\pm 0.1} \approx \pm 2e/nm^2$, $\sigma_{\pm 0.15} \approx \pm 3e/nm^2$, $\sigma_{\pm 0.2} \approx \pm 4e/nm^2$. With these surface charge densities, the atoms on the NP surface had the partial charges of $\pm 0.05e$, $\pm 0.1e$, $\pm 0.15e$ and $\pm 0.2e$, respectively. Using MD modeling data, radial distributions of the mean polypeptide atom density with differentiation by the types of units were calculated with respect to all obtained conformations on the final stationary path segment.

Figure 4, a shows the conformational structure of polypeptide P1 on the surface of the spherical neutral gold NP. It can be seen that a dense polyampholyte crown is formed on the NP surface and envelopes the whole NP with adsorption of the polypeptide amino-acid residues on the surface regardless of their type. A similar picture was also observed for other given polypeptides.

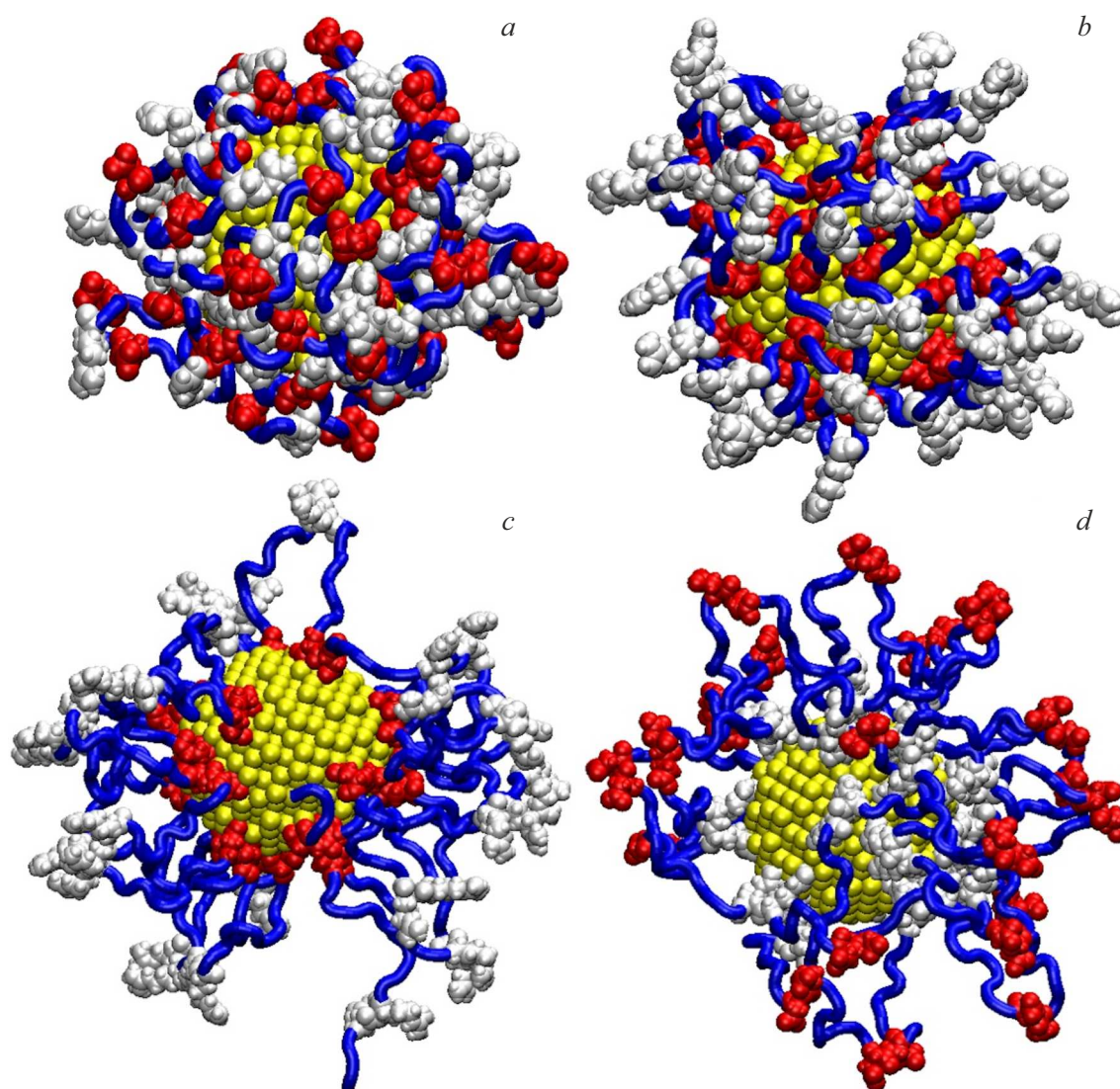


Figure 4. Polypeptides P1 (*a, b*) and P3 (*c, d*) after MD modeling on the neutral gold NP (*a*) and on the charged gold NP with the surface charge density $\sigma_{+0.2}$ (*b, c*) and $\sigma_{-0.2}$ (*d*), respectively (blue tube — Ala units, white — Arg units, red — Asp units, yellow — NP).

Figure 5, *a* shows the radial distributions of the mean atom density of the polypeptide P1 on the neutral NP surface with differentiation by the types of units. Typical radial distributions of the mean polypeptide atom density were formed with a radial density peak at the NP surface for all amino-acid residues.

Figure 4, *b–d* shows the conformational structures of the polyampholyte polypeptides P1 and P3 obtained using the MD modeling data on the surface of the charged spherical gold NP. As the absolute surface density of electric charge on the NP surface increased, the polyampholyte crown structure enveloping the spherical NP changed considerably. The polyampholyte units with the charge of opposite sign with respect to the NP charge were arranged on the surface and the units with the same sign as that of the surface were getting farther to the periphery as the surface charge density

increased. Beginning from the surface charge density $\sigma_{\pm 0.15}$ and $\sigma_{\pm 0.2}$, all like-charged amino-acid residues with respect to the NP surface were shifted from NP as far as possible at a distance defined by the number of neutral units between the unlike-charged units in the macrochain. A volume occupied by the polyampholyte crown increased considerably.

At the maximum given surface charge densities, an ordered conformational structure of the adsorbed polyampholyte was formed on the charged NP surface and consisted of three layers: two unlike-charged layers and one neutral layer between them. This can be seen on the radial dependences of the mean atom density of the polypeptide P1 with the NP surface charge densities $\sigma_{+0.2}$ (Figure 5, *b*) and $\sigma_{-0.2}$ (Figure 5, *c*). It can be seen that the radial distribution profiles of the mean atom density

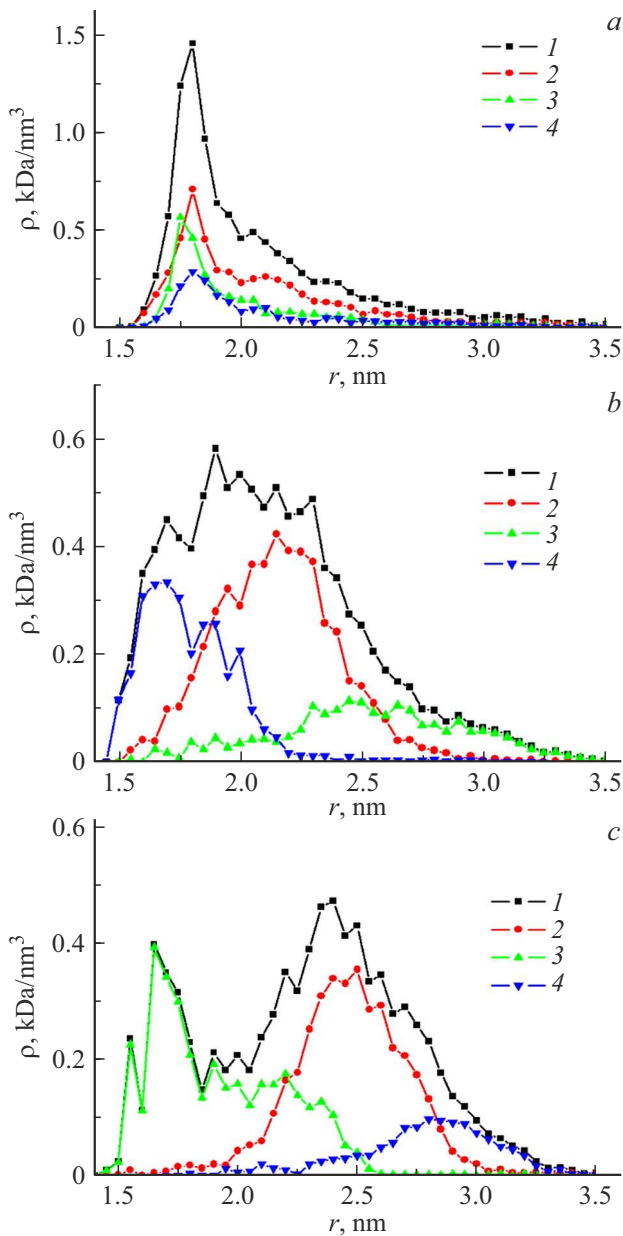


Figure 5. Radial dependences of the mean atom density of the polypeptide P1 on the neutral (a), positively and negatively charged spherical gold NP with the surface charge density $\sigma_{+0.2}$ (b) and $\sigma_{-0.2}$ (c). 1 — dependence of the mean density with respect to all polypeptide atoms; 2, 3 and 4 — averaged densities for the types of Ala, Arg and Asp amino-acid residues.

of different amino-acid residues are displaced with respect to one another, and the radial mean density distributions themselves differ considerably from those for the neutral surface (Figure 5, a). A positively charged NP has a layer of negatively charged Asp amino-acid residues near its surface (Figure 4, b and c), neutral Ala units in the middle and positively charged Arg amino-acid residues on the periphery (Figure 5, b). For the negatively charged NP surface (Figure 1, d), a mirrored arrangement of the amino-acid residue layers is observed (Figure 5, c). Figure 5, b and c

shows swelling of the enveloping crown throughout the spherical NP surface. The polyampholyte crown thickness on the maximally charged surface of the spherical metallic NP was the higher, the greater the number of neutral units between the unlike-charged residues in the macrochain was, and it was equal for the polypeptide P1 to about 2 nm, for the polypeptide P2 — to about 2.5 nm, for the polypeptide P3 — to about 4 nm, and for the polypeptide P4 — to about 5 nm.

Two-particle „molecule-NP“ system luminescence

An electron-excited molecule with the transition dipole moment $\mathbf{p}_0 = \langle i | e \delta \mathbf{r} | f \rangle$ fixed on the macrochain and spaced away from the center of the spherical NP with a radius of R at a distance of $r > R$ creates an inhomogeneous field with the following potential in the point with spherical coordinates inside NP

$$\delta\varphi(r'; \theta; r, \vartheta) = -p_0 \cos \vartheta \sum_{l=0}^{\infty} \frac{(2l+1)(l+1)}{l\varepsilon(\omega) + (l+1)\varepsilon_2} \frac{(r')^l}{r^{l+2}} P_l(\cos \theta), \quad r' < R. \quad (9)$$

In equation (9), $P_l(\cos \theta)$ is the l -th order Legendre polynomial; ϑ is the angle between the vectors \mathbf{p}_0 and \mathbf{r} ; $\varepsilon(\omega)$ is the dielectric permittivity of the NP metal at the frequency ω ; ε_2 is the solvent permittivity.

The inhomogeneous field of the dipole \mathbf{p}_0 induces a dipole moment in NP

$$\mathcal{P}(\omega | r, \vartheta) = -\frac{1}{2\varepsilon_2} \int_0^R \int_0^\pi [\varepsilon(\omega) - \varepsilon_2] \times \nabla \delta\varphi(r', \theta; r, \vartheta) r'^2 dr' \sin \theta d\theta, \quad (10)$$

whose value depends on the orientation of the vector \mathbf{p}_0 and the distance r between the NP center and the molecule.

Thanks to the plasmonic assistance, spontaneous transitions with the photon radiation will occur faster due to the presence of a nanoantenna-particle near the excited molecule [28]. The spontaneous transition rate $w_{sp}(\omega | r, \vartheta)$ at the frequency ω is written as

$$w_{sp}(\omega | r, \vartheta) = \frac{4}{3} \frac{\omega^3}{\hbar c^3} |\mathbf{p}_0 + \mathcal{P}(\omega | r, \vartheta)|^2. \quad (11)$$

A part of the electromagnetic field energy dissipates in NP due to the presence of the imaginary part $\text{Im}\varepsilon(\omega)$ of the metal permittivity and then the rate of nonradiative electron excitation transfer from the molecule to the metallic globule

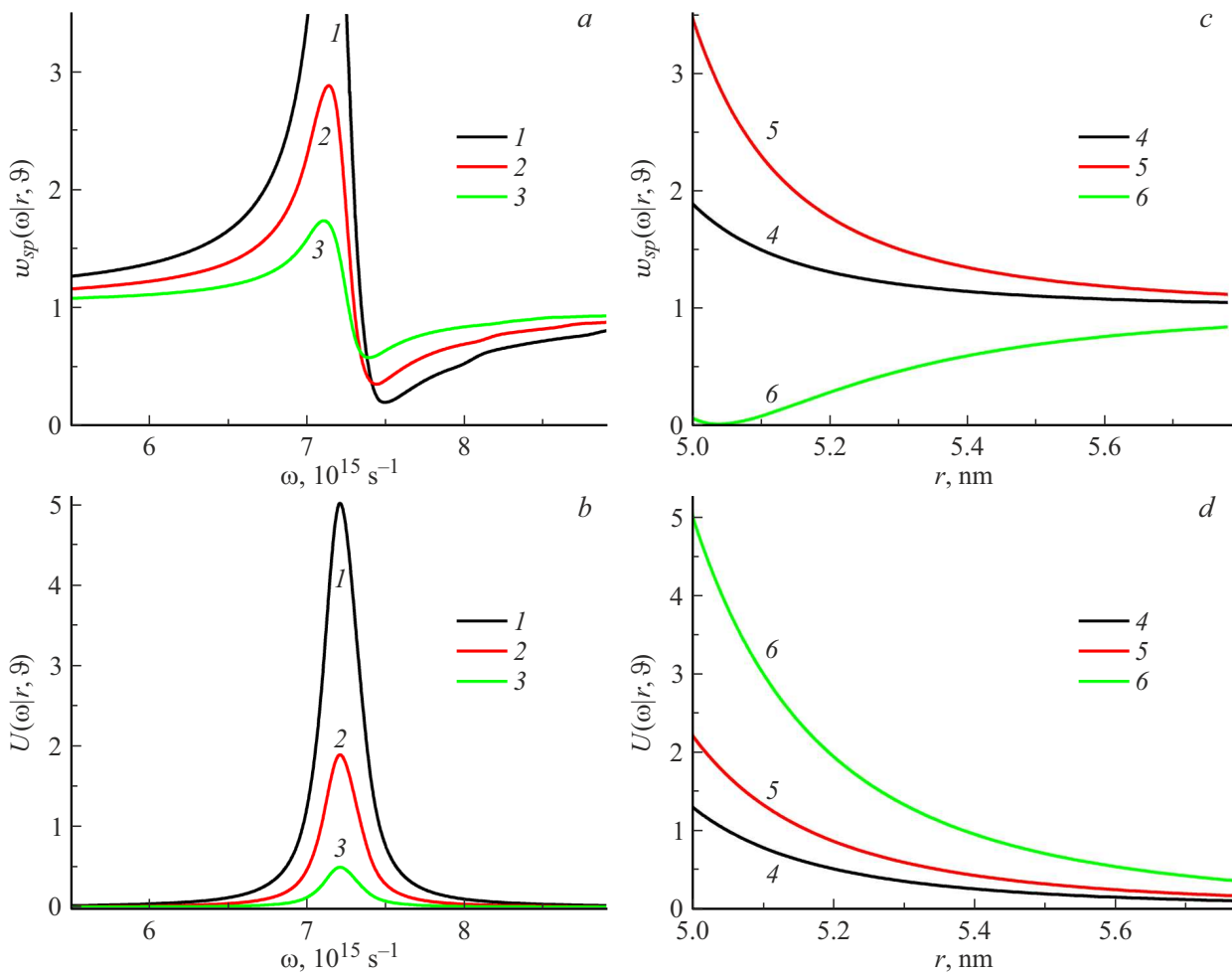


Figure 6. Frequency (*a, b*) and radial (*c, d*) dependences of the spontaneous transition probability (*a, c*) and nonradiative energy transfer rate (*b, d*) in the „molecule-NP“ system related to the transition probability without NP at the distances between the molecule and the center of NP: 1 – 5.2 nm, 2 – 5.4 nm, 3 – 5.8 nm and at the frequencies 4 – $6.8 \cdot 10^{15} \text{ c}^{-1}$, 5 – $7.0 \cdot 10^{15} \text{ c}^{-1}$, 6 – $7.2 \cdot 10^{15} \text{ c}^{-1}$. $R_{\text{NP}} = 5 \text{ nm}$, $\omega_{\text{pl}} = 7.2 \cdot 10^{15} \text{ c}^{-1}$, $\vartheta = 0$.

may be written as

$$U(\omega|r, \vartheta) = \frac{1}{2\hbar} \int_0^R \int_0^\pi \text{Im}\varepsilon(\omega) \times |\nabla\delta\varphi(r', \theta; r, \vartheta)|^2 r'^2 dr' \sin\theta d\theta. \quad (12)$$

Then the local luminescence intensity of a single molecule on a chain spaced away from the center of NP at a distance r will be defined by expression [29]

$$I_1(\omega|r, \vartheta) = \frac{1}{2\pi} \frac{w_{sp}^2(\omega|r, \vartheta)\Gamma(\omega|r, \vartheta)}{(\omega - \omega_{if})^2 + \Gamma^2(\omega|r, \vartheta)},$$

$$\Gamma(\omega|r, \vartheta) = w_{sp}(\omega|r, \vartheta) + U(\omega|r, \vartheta) + K, \quad K = \text{const}. \quad (13)$$

Here, $\Gamma(\omega|r, \vartheta)$ is the spectral width of the M-NP two-particle system radiation line at the frequency ω .

The frequency dependence $w_{sp}(\omega|r, \vartheta)$ of the spontaneous transitions in the „molecule-NP“ system related

to the transition probability w_0 without NP is shown in Figure 6, *a*. $w_{sp}(\omega|r, \vartheta)$ has a non-monotonic behavior: in a frequency range lower than the plasmonic resonance frequency ($\omega < \omega_{pl}$), transition rate acceleration takes place and achieves its peak near the resonance $\omega \approx \omega_{pl}$, and the spontaneous transition probability $w_{sp}(\omega|r, \vartheta)$ at the frequencies $\omega > \omega_{pl}$ decreases significantly.

This trend also appears in the field structure induced in NP: with $\omega > \omega_{pl}$ the field strength vector orientation varies from point to point within NP. This is due to the fact that the electron plasma oscillations cannot „keep pace with“ the external field oscillation frequency of the excited molecule and a phase shift occurs between them. Frequency dependence of the rate of nonradiative electron excitation transfer from the molecule to NP (Figure 6, *b*) is a resonance peak with its maximum at $\omega \approx \omega_{pl}$ whose amplitude expectedly drops as the distance between the molecule and NP grows. Figure 6, *c–d* shows that the radial dependence of the nonradiative electron excitation

energy transfer from the molecule to NP decreases with the increase in the radius much faster than the dependence of the spontaneous transition probability in the „molecule-NP“ system.

Luminescence quantum yield of the isolated „molecule-NP“ pair that defines the local luminescence intensity $I_1(r)$ in (4) and (13) may be given by expression

$$\eta(\omega|r, \vartheta) = \frac{w_{sp}(\omega|r, \vartheta)}{w_{sp}(\omega|r, \vartheta) + U(\omega|r, \vartheta) + K}.$$

In case when the spectral line width of the „molecule-NP“ system radiation is small and its frequency peak is close to the NP plasmonic resonance frequency, luminescent signal in the line peak $I_1(\omega_{if}|r, \vartheta)$ may be used instead of the spectral characteristic of the luminescent signal intensity $I(\omega|r, \vartheta)$ (13).

The resultant luminescent signal from an individual charged plasmonic NP with the dyed polymer chain adsorbed on its surface will be defined by the following expression

$$I \sim \int_R^\infty I_1(r)n(r)4\pi r^2 dr \sim 4\pi \int_R^{r_0} I_1(r)[F_0^I(r)]^2 r^2 dr + 4\pi \int_{r_0}^\infty I_1(r)[F_0^{II}(r)]^2 r^2 dr.$$

Expression (10)–(11) suggests that the radiative transition probability is defined by the complex-valued function module $\varepsilon(\omega)$ and real part, and the nonradiative transition rate is defined by the imaginary part $\text{Im}\varepsilon(\omega)$, i.e. by the electronic conductivity of the NP material. Then different radial dependences $I_1(r)$ may be obtained for different ratios of the radiative and nonradiative channels. For a metal with high field decay near the NP surface, the nonradiative channel will prevail and the luminescence intensity will decrease (Figure 7, curve 1), on the contrary, when the field oscillation decay in NP is low, luminescence increase is observed near the NP surface (Figure 7, curve 2). A non-monotonic dependence may take place at an intermediate rate ratio (Figure 7, curve 3).

As shown above, the NP charge plays a role of a factor governing the adsorbed polyampholyte chain architecture and photochrome molecule distribution near NP. Consequently, the ratio between the efficiencies of the radiative and nonradiative molecule deactivation channels and, accordingly, the resultant luminescence intensity of the „dyed polyampholyte chain-NP“ system will vary.

The calculations show that the desired dependences in case of prevalence of the nonradiative molecule deactivation channel near NP (Figure 8, curves 1, 2, 3) or prevalence of the radiative channel near NP (Figure 8, curve 4, 5, 6) have mutually opposing behavior: the luminescence intensity steadily reduces in the first case and grows in the second case.

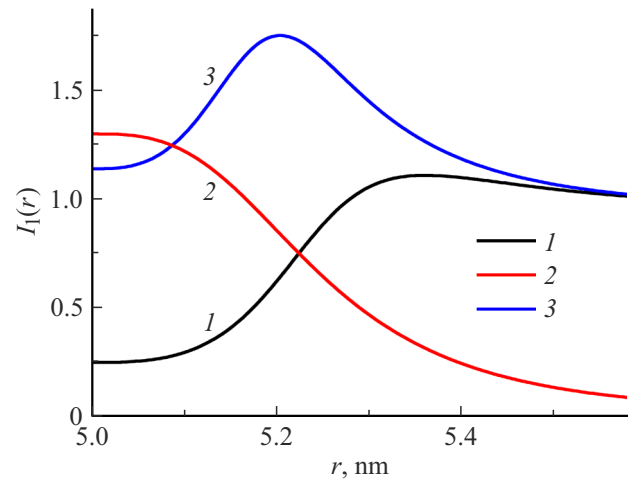


Figure 7. Radial dependence of the „molecule-NP“ luminescence intensity at various ratios of radiative and nonradiative deactivation channels.

For different calculation models of the density of chain units, the amplitude of the effect in question is different, therefore, its mechanisms may be analyzed in more detail. Thus, the modulation depth for the analytical model based on equations (6)–(8) is minimal (Figure 8, curves 2, 5) and is associated only with compacting of $n(r)$. Note that, despite the fact that variation of this distribution in the near-surface region ($R < r < r_0$) and peripheral region ($r > r_0$), the latter defines the sign of the effect due to its larger volume.

Calculations in the Boltzmann approximation (Figure 8, curves 1, 4) and according to the formal approach on the basis of equations (4)–(5) (Figure 8, curves 3, 6) give a considerably higher effect. This is because the shift of the radial density distribution towards the plasmonic NP is expressly considered, besides the polymer crown compacting mechanism with a phytochrome in the potential well $V_{9-3}^{pQ}(r) = V_{9-3}(r) + V_{pQ}(r)$.

Conclusion

The study addresses the effect of the spherical plasmonic NP on the conformational structure of polypeptides adsorbed on its surface and the luminescence of molecules associated with the polymer molecule. The proposed mathematical model is used to analyze the influence of the plasmonic NP charge on the parameters of the adsorption potential, and it is shown that the potential valley moves slightly towards the NP surface with charge growth, whereas the potential well depth increases. Distributions of the polymer chain unit density in the NP near-surface layer are calculated depending on the NP charge using several models: quasi-point freely articulated unit model (Boltzmann approximation), original model version based on the Grosberg-Khokhlov equation solution and formal approach combining both models. It is shown that, as

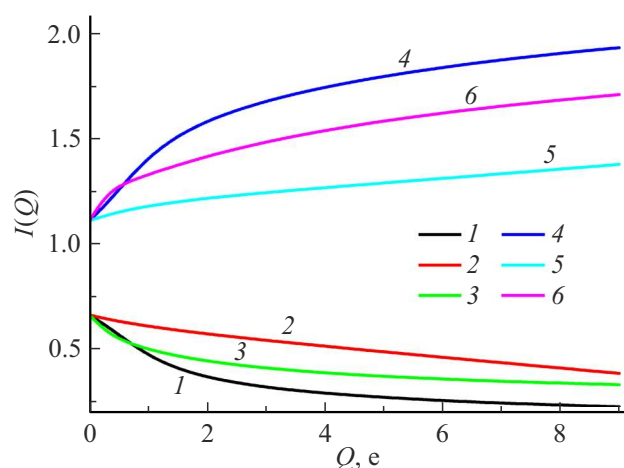


Figure 8. Dependence of the „dye polyampholyte chain-NP“ luminescence intensity on the NP charge. 1, 4 — the Boltzmann approximation; 2, 5 — the analytical model according to equations (6); 3, 6 — formal approach according to equations (4). 1, 2, 3 — nonradiative channel dominance near NP; 4, 5, 6 — radiative channel dominance near NP.

the NP charge increases, the polyampholyte chain unit distribution becomes more compact and displacement of the unit distribution peak towards the NP surface is observed in the Boltzmann approximation and the formal model.

Moreover, MD modeling of the polyampholyte polypeptide enveloping the spherical gold NP demonstrates that the polyampholyte crown swells as the absolute value of the NP charge grows. And a structured three-layer polyampholyte shell is formed depending on the sign of the macrochain unit charge. The shell is the thicker, the higher the number of the neutral units between the opposite-charged units in the macromolecule is.

Frequency and spatial dependence of the spontaneous transition probability and nonradiative energy transfer of the electron excitation in the „molecule-NP“ system are analyzed. The situation when the polymer chain units serve as linkers for photochromic centers and the NP charge plays a role of a factor governing both the polyampholyte chain architecture and the photochrome molecule distribution near the NP surface. Consequently, the ratio of the radiative and nonradiative molecule deactivation channel efficiencies and, accordingly, the luminescence intensity of the „dye polyampholyte chain-NP“ system will vary. The calculations show that the desired dependences in case of prevalence of the nonradiative molecule deactivation channel near NP or dominance of the radiative channel near NP have mutually opposing behavior: the luminescence intensity steadily reduces in the first case and grows in the second case.

Funding

The study was supported by the Ministry of Science and Higher Education of the Russian Federation: State Order 2024 for research № FSGU-2023-0003 and Grant for major

research projects in priority research and development areas № 075-15-2024-550.

Conflict of interest

The authors declare that they have no conflict of interest.

References

- [1] C. Boyer, M.R. Whittaker, K. Chuah, J. Liu, T.P. Davis. *Langmuir*, **26**, 2721 (2010). DOI: 10.1021/la902746v
- [2] F. Yi, X. Huang, *J. Ren. Anal. Chem.*, **90**, 3871 (2018). DOI: 10.1021/acs.analchem.7b04569
- [3] N.N. Heris, L. Baghani, F. Khonsari, R. Varshochian, R. Dinariyand, F. Atyabi. *Journal of Drug Delivery Science and Technology*, **87**, 104869 (2023). DOI: 10.1016/j.jddst.2023.104869
- [4] Z. Jin, J. Yeung, J. Zhou, M. Retout, W. Yim, P. Fajtová, B. Gosselin, I. Jabin, G. Bruylants, H. Mattoussi, A.J. O'Donoghue, J.V. Jokerst. *ACS Appl. Mater. Interfaces*, **15**, 20483 (2023). DOI: 10.1021/acsami.3c00862
- [5] K.M. Greskovich, K.M. Powderly, M.M. Kincanon, N.B. Forney, C.A. Jalomo, A. Wo, C.J. Murphy. *Acc. Chem. Res.*, **56**, 1553 (2023). DOI: 10.1021/acs.accounts.3c00109
- [6] D.L. Amarasekara, C.S. Kariyawasam, M.A. Hejny, V.B. Torgall, T.A. Werfel, N.C. Fitzkee. *ACS Appl. Mater. Interfaces*, **16**, 4321 (2024). DOI: 10.1021/acsami.3c13288
- [7] Z. Jin, N. Dridi, G. Palui, V. Palomo, J.V. Jokerst, P.E. Dawson, Q.A. Sang, H. Mattoussi. *J. Am. Chem. Soc.*, **145**, 4570 (2023). DOI: 10.1021/jacs.2c12032
- [8] T. Chiang, H. Hsiao. *Talanta*, **253**, 123913 (2023). DOI: 10.1016/j.talanta.2022.123913
- [9] N.Yu. Kruchinin, M.G. Kucherenko. *Surfaces and Interfaces*, **27**, 101517 (2021). DOI: 10.1016/j.surfin.2021.101517
- [10] N.Yu. Kruchinin, M.G. Kucherenko. *Colloid Journal*, **83**, 591 (2021). DOI:10.1134/S1061933X21050070
- [11] N.Yu. Kruchinin, M.G. Kucherenko. *Colloid Journal*, **84**, 169 (2022). DOI: 10.1134/S1061933X22020077
- [12] M.G. Kucherenko, N.Yu. Kruchinin, P.P. Neyasov. *Eurasian Physical Technical Journal*, **19**, 19 (2022). DOI: 10.31489/2022No2/19-29
- [13] N.Yu. Kruchinin, M.G. Kucherenko. *High Energy Chemistry*, **56**, 499 (2022). DOI: 10.1134/S0018143922060108
- [14] N.Yu. Kruchinin, M.G. Kucherenko. *Polymer Science Series A*, **65** (2), 224 (2023). DOI: 10.1134/S0965545X23700815
- [15] A.S. de Dios, M.E. Díaz-García. *Analytica Chimica Acta*, **666**, 1 (2010). DOI: 10.1016/j.aca.2010.03.038
- [16] I. Pastoriza-Santos, C. Kinnear, J. Pérez-Juste, P. Mulvaney, L.M. Liz-Marzán. *Nature Rev. Mater.*, **3**, 375 (2018). DOI: 10.1038/s41578-018-0050-7
- [17] V.V. Klimov. *Nanoplazmonika* (Fizmatlit, Moskva, 2009) (in Russian).
- [18] N.Kh. Ibrayev, M.G. Kucherenko, D.A. Temirbayeva, E.V. Seliverstova. *Opt. Spectrosc.*, **130** (5), 721 (2022). DOI: 10.21883/EOS.2022.05.54441.1-22
- [19] A.Yu. Grosberg, A.R. Khokhlov. *Statisticheskaya fizika makromolekul* (Nauka, Moskva, 1989) (in Russian).
- [20] S.F. Edvards. *Proc. Phys. Soc.*, **85**, 613 (1965).
- [21] M.G. Kucherenko, T.M. Chmereva. *Vestnik OGU*, (9), 177 (2008) (in Russian).
- [22] M.G. Kucherenko, N.Yu. Kruchilin, T.M. Chmereva. *Vestnik OGU*, (5), 124 (2010) (in Russian).

- [23] J.C. Phillips, R. Braun, W. Wang, J. Gumbart, E. Tajkhorshid, E. Villa, C. Chipot, R.D. Skeel, L. Kale, K. Schulten. *J. Comput. Chem.* **26**, 1781 (2005). DOI: 10.1002/jcc.20289
- [24] A.D. Jr. MacKerell, D. Bashford, M. Bellott, Jr. R.L. Dunbrack, J.D. Evanseck, M.J. Field, S. Fischer, J. Gao, H. Guo, S. Ha, D. Joseph-McCarthy, L. Kuchnir, K. Kuczera, F.T.K. Lau, C. Mattos, S. Michnick, T. Ngo, D.T. Nguyen, B. Prodhom, W.E. Reiher III, B. Roux, M. Schlenkrich, J.C. Smith, R. Stote, J. Straub, M. Watanabe, J. Wiorcikiewicz-Kuczera, D. Yin, M. Karplus. *J. Phys. Chem. B*, **102**, 3586 (1998). DOI: 10.1021/jp973084f
- [25] H. Heinz, R.A. Vaia, B.L. Farmer, R.R. Naik. *J. Phys. Chem. C*, **112**, 17281 (2008). DOI: 10.1021/jp801931d CCC: 40.75
- [26] T. Darden, D. York, L. Pedersen. *J. Chem. Phys.*, **98**, 10089 (1993). DOI: 10.1063/1.464397
- [27] W.L. Jorgensen, J. Chandrasekhar, J.D. Madura, R.W. Impey, M.L. Klein. *J. Chem. Phys.*, **79**, 926 (1983). DOI: 10.1063/1.445869
- [28] V.V. Klimov, M. Dyuklua, V.S. Letokhov. *Kvant. elektron.*, **31**(7), 569 (2001) (in Russian). DOI: 10.1070/QE2001v031n07ABEH002007
- [29] M.G. Kucherenko, I.R. Alimbekov, P.P. Neyasov. *Khimicheskaya Fizika i Mezoskopiya*, **23**(3), 272 (2021). DOI: 10.1134/S106378422209002X

Translated by E.Ilinskaya